http://dx.doi.org/10.5012/bkcs.2013.34.12.3553

3D-QSAR Studies on Chemical Features of 3-(benzo[*d*]oxazol-2-yl)pyridine-2-amines in the External Region of c-Met Active Site

Joo Yun Lee,[†,§] Kwangho Lee,[‡] Hyoung Rae Kim,[‡] and Chong Hak Chae[§,*]

[†]*Department of Chemistry, Chungbuk National University, Cheongju, Chungbuk 361-763, Korea*
[‡]*Bio-Organic Science Division, Korea Research Institute of Chemical Technology, Daejeon 305-600, Korea*
[§]*Drug Discovery Platform Technology Team, Korea Research Institute of Chemical Technology, Daejeon 305-600, Korea*
[*]*E-mail: chchae@krict.re.kr*
Received May 1, 2013, Accepted September 4, 2013

The three dimensional-quantitative structure activity relationship (3D-QSAR) studies on chemical features of pyridine-2-amines in the external region of c-Met active site (ER chemical features of pyridine-2-amines) were conducted by docking, comparative molecular field analysis (CoMFA), and topomer CoMFA methods. The CoMFA model obtained the partial least-squares (PLS) statistical results, cross-validated correlation coefficient (q^2) of 0.703, non cross-validated correlation coefficient (r^2) of 0.947 with standard error of estimate (SEE) of 0.23 and the topomer CoMFA obtained q^2 of 0.803, r^2 of 0.940, and SEE of 0.24. Further, the test set was applied to validate predictive abilities of models, where the predictive r^2 (r^2_{pred}) for CoMFA and topomer CoMFA models were 0.746 and 0.608, respectively. Each contribution of ER chemical features of pyridine-2-amines to the inhibitory potency showed correlation coefficients, r^2 of 0.670 and 0.913 for two core parts, 3-(benzo[*d*]oxazol-2-yl)pyridine-2-amine and 3-(1-(2,6-dichloro-3-fluorophenyl)ethoxy) pyridine-2-amine, respectively, with corresponding experimental pIC_{50}.

Key Words : c-Met inhibitor, Pyridine-2-amines, 3D-QSAR, CoMFA, Topomer CoMFA

Introduction

The c-Met (mesenchymal-epithelial transition factor) and its ligand hepatocyte growth factor (HGF), also called scatter factor, are attractive targets for the cancer therapy. Normal HGF/c-Met signaling plays an important role during embryogenesis and tissue injury repair, but aberrant signaling correlates with aggressive tumor growth and poor prognosis in cancer patients. Different approaches to inhibition of HGF/c-Met signaling pathway include antagonistic ligands and antibodies against either HGF or c-Met.[1-8] Particulary, small molecule inhibitors of c-Met have been reported in experimental and computational literature.[9-15]

Asses *et al.* proposed that binding modes of ligands in c-Met involve seven structurally-distinct areas based on the analyses of interaction energies on ligand-protein complexes.[10] Larsen *et al.* studied orientations of tea catechins as c-Met inhibitor by molecular docking studies.[11] Caballero *et al.* performed docking studies of 3-fluoro-4-(pyrrolo[2,1-*f*][1,2,4]triazin-4-yloxy)anilines (FPTA), 3-fluoro-4-(1*H*-pyrrolo[2,3-*b*]pyridin-4-yloxy) anilines (FPPA), and 4-(4-amino-2-fluorophenoxy)-2-pyridinylamines (AFPP) in c-Met.[12] They suggested that binding sites of ligand-enzyme complexes include five regions: scaffold region, external region, central region, allosteric site I, and allosteric site II. Also, they analyzed how different chemical features of three series, FPTA, FPPA, and AFPP in each identified region contribute to their inhibitory potencies.

As part of our effort toward developing an effective therapeutic agent for c-Met inhibitors, we identified 3-(benzo[*d*]oxazol-2-yl)pyridine-2-amines as orally active c-Met inhibitors, which were focused on structural modification of substituents located in the external region of c-Met active site.[13] The backbone traces of external region, Lys1161-His1162-Gly1163-Asp1164-Leu1165-Arg1166-Asn1167 and Asn1209-Cys1210-Met1211-Leu1212-Asp1213-Glu1214-Lys1215-Phe1216-Thr1217-Val1218-Lys1219-Val1220-Ala1221 are highly conserved because of hydrogen bonding networks, where is better for studies on structure-activity relationship of c-Met inhibitors than in flexible other regions. In the present study, the three dimensional-quantitative structure activity relationship (3D-QSAR) studies on chemical features of 3-(benzo[*d*]oxazol-2-yl)pyridine-2-amines in the external region of c-Met active site were conducted to identify chemical features essential for enhancing their inhibitory potencies using docking, comparative molecular field analysis (CoMFA), and topomer CoMFA methods.

Methods

Data Set. By adding 3-(1-(2,6-dichloro-3-fluorophenyl)-ethoxy)pyridine-2-amines[15] to 3-(benzo[*d*]oxazol-2-yl)pyridine-2-amines,[13] the data set were enough to be used in 3D-QSAR studies on chemical features of pyridine-2-amines in the external region of c-Met active site (abbreviation: ER chemical features of pyridine-2-amines).

The activities of 3-(1-(2,6-dichloro-3-fluorophenyl)ethoxy)-pyridine-2-amines, K_i values were converted into IC_{50} values using the equation by Copeland *et al.*,[16] $K_i = IC_{50}/(S/K_m+1)$ with the total concentrations of substrate (S) of 100

Table 1. Molecular structures of the pyridine-2-amines and their experimental, predictive activities, and R1 contributions

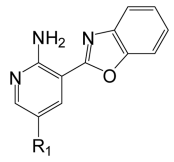

Comps[a]	R1	$pIC_{50,exp}$[b]	$pIC_{50,CoM}$[b]	$pIC_{50,Topo}$[b]	R1[c]
1*	Phenyl	5.00	5.16	4.78	1.11
2*	4-Pyridyl	5.28	5.23	4.99	1.32
3	3-Pyridyl	5.00	5.06	4.56	0.89
4	[1-methyl-1*H*-pyrazole]-4-yl	5.68	5.83	5.61	1.95
5	[2-(1*H*-pyrazol-1-yl)ethan-1-ol]-4-yl	5.89	6.05	5.88	2.21
6	[1-(tetrahydro-2*H*-pyran-4-yl)-1*H*-pyrazole]-4-yl	6.37	6.50	6.26	2.59
7*	[4-(1*H*-pyrazol-1-yl)piperidine]-4-yl	7.10	6.44	6.23	2.56
8*	[1-(4-(1*H*-pyrazol-1-yl)piperidin-1-yl)ethan-1-one]-4-yl	8.52	7.20	6.16	2.49
9	[1-(4-(1*H*-pyrazol-1-yl)piperidin-1-yl)propan-1-one]-4-yl	8.15	7.65	7.23	3.57
10	[(4-(1*H*-pyrazol-1-yl)piperidin-1-yl)(phenyl)methanone]-4-yl	6.85	6.89	6.83	3.17
11	[1-(4-(1*H*-pyrazol-1-yl)piperidin-1-yl)-2-methoxyethan-1-one]-4-yl	7.77	7.80	7.47	3.81
12	[1-(4-(1*H*-pyrazol-1-yl)piperidin-1-yl)-2-(dimethylamino)ethan-1-one]-4-yl	7.22	7.12	7.29	3.62
13	[*N*,*N*-diethyl-4-(1*H*-pyrazol-1-yl)piperidine-1-carboxamide]-4-yl	6.45	6.50	6.91	3.24
14*	[methyl 4-(1*H*-pyrazol-1-yl)piperidine-1-carboxylate]-4-yl	7.24	7.02	6.88	3.21
15	[1-(methylsulfonyl)-4-(1*H*-pyrazol-1-yl)piperidine]-4-yl	6.43	6.42	6.15	2.48
16*	[1-(4-(1*H*-pyrazol-1-yl)piperidin-1-yl)-2-hydroxyethan-1-one]-4-yl	7.59	7.54	7.47	3.81

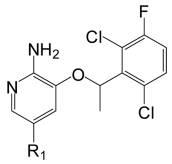

Comps[a]	R1	$pIC_{50,exp}$[b]	$pIC_{50,CoM}$[b]	$pIC_{50,Topo}$[b]	R1[c]
17	H	4.70	4.54	4.60	0.03
18	Br	4.74	4.69	4.73	0.17
19	CN	4.68	4.74	4.89	0.33
20	-NHCOPh	5.26	5.42	4.94	0.37
21*	Phenyl	5.55	5.90	5.68	1.11
22	[(*R*)-phenyl(2-(pyrrolidin-1-ylmethyl)pyrrolidin-1-yl)methanone]-4-yl	7.52	7.68	6.93	2.36
23*	[phenyl(4-(pyrrolidin-1-yl)piperidin-1-yl)methanone]-4-yl	7.00	7.02	6.24	1.67
24	[*N*-(2-(pyrrolidin-1-yl)ethyl)benzamide]-4-yl	6.68	6.70	6.27	1.70
25	[((3*S*,5*R*)-3,5-dimethylpiperazin-1-yl)(phenyl)methanone]-4-yl	6.96	6.85	6.28	1.71
26	[1*H*-pyrazole]-1-yl	5.05	5.54	4.82	0.25
27	[1-methyl-1*H*-imidazole]-4-yl	6.17	5.99	5.86	1.29
28*	[thiazole]-2-yl	5.66	5.56	5.35	0.78
29	[isoxazole]-4-yl	6.25	5.69	6.18	1.61
30	[1*H*-pyrazole]-5-yl	6.01	5.68	5.89	1.32
31*	[1*H*-pyrazole]-4-yl	6.64	5.39	6.11	1.54
32	[3,5-dimethyl-1*H*-pyrazole]-4-yl	6.19	6.33	6.19	1.62
33*	[1-methyl-1*H*-pyrazole]-4-yl	6.89	6.51	6.51	1.95
34	[1-isobutyl-1*H*-pyrazole]-4-yl	7.00	6.97	6.89	2.33
35	[*N*-(2-(dimethylamino)ethyl)-2-methyl-2-(1*H*-pyrazol-1-yl)propanamide]-4-yl	6.77	6.68	6.33	1.77
36	[*N*-(2-(dimethylamino)ethyl)-2-(1*H*-pyrazol-1-yl)acetamide]-4-yl	6.85	6.81	6.57	2.00
37	[4-((1*H*-pyrazol-1-yl)methyl)tetrahydro-2*H*-pyran-4-ol]-4-yl	6.89	7.08	6.79	2.22
38	[1-(azetidin-3-ylmethyl)-1*H*-pyrazole]-4-yl	6.70	7.01	6.93	2.36
39	[2-(3-((1*H*-pyrazol-1-yl)methyl)azetidin-1-yl)acetamide]-4-yl	7.15	7.09	7.04	2.47
40	[1-(azetidin-3-yl)-1*H*-pyrazole]-4-yl	7.00	7.16	6.73	2.16
41*	[(*S*)-1-(pyrrolidin-3-yl)-1*H*-pyrazole]-4-yl	7.15	6.92	7.00	2.43
42*	[3-(1*H*-pyrazol-1-yl)piperidine]-4-yl	7.40	7.21	7.08	2.51
43*	[1-(tetrahydro-2*H*-pyran-4-yl)-1*H*-pyrazole]-4-yl	6.96	7.15	7.16	2.59
44[e]	[4-(1*H*-pyrazol-1-yl)piperidine]-4-yl	7.30	7.23	7.13	2.56

[a]The compounds with "*" are included in the test set. [b]$pIC_{50,exp}$ values are experimental inhibitory activities. $pIC_{50,CoM}$ and $pIC_{50,Topo}$ values are inhibitory activities predicted by CoMFA and topomer CoMFA models, respectively. [c]R1 value means the level of contribution of R1 fragment of compound to inhibitory activities.

uM and the Michaelis constant for the substrate (K_m) of 56 uM[15] and then all IC_{50} values were also converted into pIC_{50} values using the formula pIC_{50} = 6-log[IC_{50}(uM)]. The 44 compounds having pIC_{50} values between 4.68 and 8.52 against c-Met were divided into a training set (30 compounds) and a test set (14 compounds) by the Diverse Molecules protocol of Pipeline Pilot[17] in Table 1.

Docking Analysis. All computational calculations for molecular docking were performed using the Schrödinger suite 2013.[18] The X-ray crystal structure of c-Met (PDB ID 2WGJ)[15] was revised by the Protein Preparation Wizard in Maestro v9.4 and the low-energy 3D structures of 44 compounds were generated by the LigPrep v2.6. Further, docking study was carried out with a grid box of 30 × 30 × 30 Å^3 centered on the corresponding ligand and the OPLS_2005 force field[19] using the Standard Precision (SP) protocol in Glide v5.9.[20-22]

3D-QSAR Modeling. All calculations were performed with SYBYL-X 2.0 package.[23]

CoMFA and Topomer CoMFA: Docking-based alignment was used to generate the CoMFA model. For the topomer CoMFA, each structure of data set was broken based on the number of R-groups, 2; core, R1 (red) and R2 (blue) parts as shown in Figure 4. Once fragmentation was completed, topomers were automatically standardized, normalized, and generated.

All aligned compounds or topomers were placed in a 3D cubic lattice with a grid spacing 2 Å and steric (Lennard-Jones potential) and electrostatic (Coulomb potential) fields were measured for each compound or topomer at grid points by a sp^3 hybrid carbon atom with +1 charge. Default 30 kcal/mol was used as energy cutoff to minimize domination by large steric and electrostatic field and to generate the CoMFA columns. 3D-QSAR models were represented as contour plots of variations in molecular fields (the standard deviation of the steric or electrostatic field at each grid point) multiplied by StDev*Coeff field.

In additional, the topomer CoMFA calculates the contribution of each fragment (R_n_contrib) toward the predicted activity by the sum of the contribution of that R-group to each of the four field types (positive steric, negative steric, positive electrostatic, negative electrostatic).

$$R_n\_contrib = (SE_1 \times SC_1) + (SE_2 \times SC_2) + \cdots + (SE_n \times SC_n) + (EE_1 \times EC_1) + (EE_2 \times EC_2) + \cdots + (EE_n \times EC_n)$$

where SE is the steric interaction energy calculated at a particular spatial location, SC is the coefficient of the steric term, reflecting the relative contribution of a particular spatial contribution, EE is the electrostatic interaction energy calculated at a particular spatial location, EC is the coefficient of the electrostatic term, reflecting the relative contribution of a particular spatial location, and 1, 2,⋯, n represent a particular spatial location.

Partial Least-Squares Algorithm (PLS): The PLS is one of several techniques producing an equation, or QSAR, in which the target properties, pIC_{50} values were used as dependent variables and the CoMFA descriptors were used as independent variables. When multiple dependent variables are involved, a separate QSAR equation is made for each target property but the coefficients are interrelated and generally differ from those which would be obtained analyzing the target properties one by one. PLS is an extension of the more familiar technique known as multiple regression (MR). The PLS analysis was carried out using the leave-one-out (LOO) cross-validation procedure to obtain the optimal number of components to be used subsequently in the final analysis. All cross-validated PLS analyses were performed with a column filter value of 1.0 to accelerate the regression analysis and reduce the noise. The cross-validated correlation coefficient q^2 was calculated using formula:

$$q^2 = 1 - (Y_{actual} - Y_{pred})^2/(Y_{actual} - Y_{mean})^2$$

where Y_{pred}, Y_{actual}, and Y_{mean} are predicted, actual, and mean values of the target property (pIC_{50}), respectively.

The predictive ability of 3D-QSAR models was estimated for test set using the predictive r^2 (r^2_{pred}), which is defined as:

$$r^2_{pred} = (SD - PRESS)/SD$$

where SD is the sum of squared deviations between biological activities of test set and the mean activity of training set, and PRESS is the sum of squared deviations between actual and predicted activities of test set.

Results and Discussions

Docking Analysis. The binding poses of pyridine-2-amines formed two hydrogen bonds to protein backbones, Pro1158 and Met1160 of c-Met hinge region and only showed variations in conformations of R1 parts corresponding to the external region of c-Met active site (Figure 1). R1 parts were surrounded by the side chains of Ile1084 and Tyr1159 and the backbones of Lys1161, His1162, Gly1163, and Asp 1164, where there were no interactions except for the hydrophobic interaction in our docking studies.

CoMFA. The CoMFA model obtained the PLS statistical results, cross-validated correlation coefficient (q^2) of 0.703, non cross-validated correlation coefficient (r^2) of 0.947 with the standard error of estimate (SEE) of 0.23, and F value of

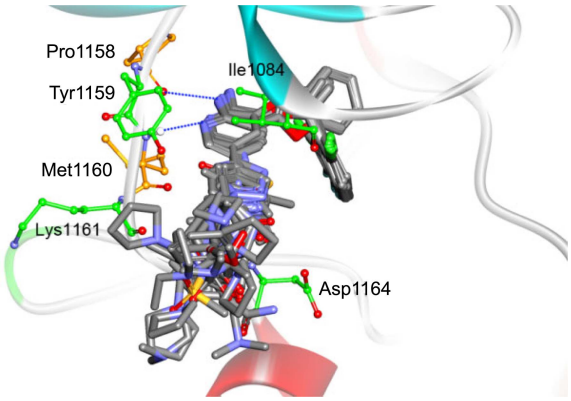

Figure 1. Alignment of all compounds docked within c-Met binding site.

Table 2. The PLS statistical restuls of CoMFA and Topomer CoMFA models

PLS statistics	CoMFA	Topomer CoMFA
q^{2a}	0.703	0.803
r^{2b}	0.947	0.940
NC[c]	4	4
F[d]	111.19	98.15
SEE[e]	0.23	0.24
r^2_{Pred}	0.746	0.608 (0.883)[f]

[a]Cross-validated correlation coefficient. [b]Non cross-validated correlation coefficient. [c]Optimal number of components. [d]F value. [e]Standard error of estimate. [f]The result without compound **8** as an outliner.

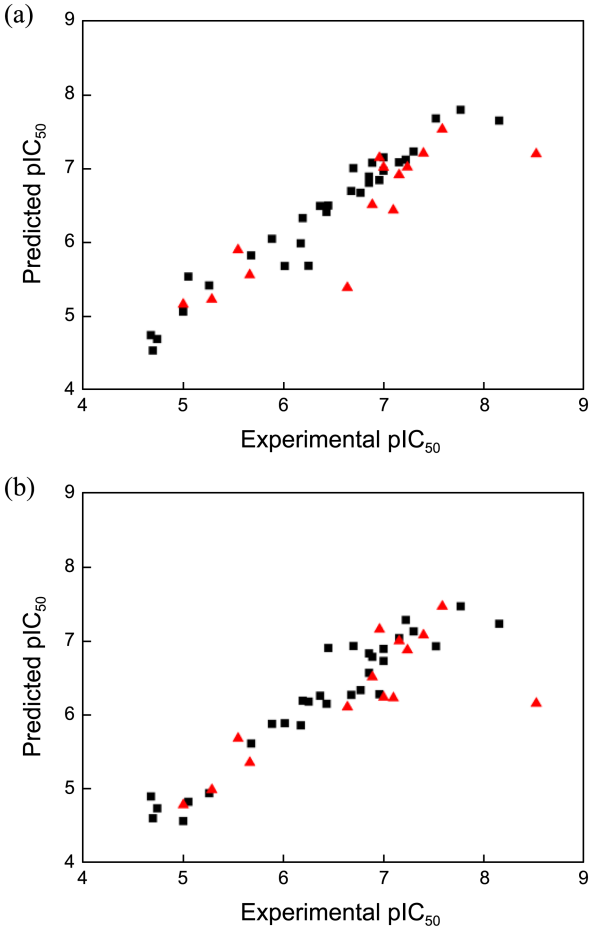

Figure 2. The correlations between their experimental and predicted activities of training (■) and test (▲) sets based on (a) CoMFA and (b) topomer CoMFA models.

111.19 using 4 components for the training set in Table 2 and predicted the test set with the predictive r^2 (r^2_{pred}) of 0.746 between their experimental and predicted pIC_{50} values (Figure 2(a)). The PLS coefficients derived from CoMFA model were displayed as steric and electrostatic contours around active compound **11** (IC_{50} = 0.017 uM) (Figure 3). Green and blue contours indicate regions where steric bulk and electronegative groups enhance the biological activity, respectively, whereas yellow and red contours indicate regions where steric bulk and electronegative groups are

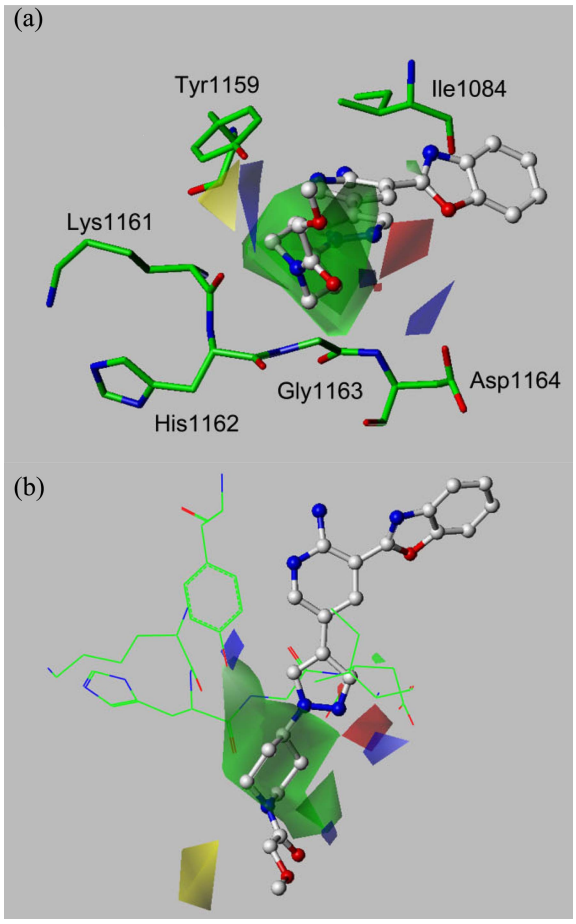

Figure 3. The contour map of CoMFA model for active compound **11** (IC_{50}, 0.017 uM) and key residues in c-Met active site. Green and yellow contours highlight favored and disfavored steric bulk groups, whereas red and blue contours highlight favored negative and positive electrostatic interactions, respectively.

detrimental to the biological activity, respectively. There were significant green contours close to piperidine ring of compound **11**, which was ascribed to the hydrophobic cleft formed by the side chains of Ile1084 and Tyr1159 and the backbones of Lys1161, His1162, Gly1163, and Asp 1164.

Topomer CoMFA. The topomer CoMFA model obtained the PLS statistical results, q^2 of 0.803, r^2 of 0.940, SEE of 0.24, and F value of 98.15 using 4 component for the training set in Table 2 and predicted the test set with r^2_{pred} of 0.608 between their experimental and predicted pIC_{50} values (Figure 2(b)). In this result, the predictive activity of compound **8** was much lower than that of compound **9** with similar chemical feature R1. If compound **8** were excluded as an outliner, the predictive ability of model could increase to r^2_{pred} of 0.883.

The R1 part occupying ribose pocket located in the external region of c-Met active site produced large green contours around piperidine ring of compound **11** and compound **3** containing the small pyridine ring on the green contour was not good as c-Met inhibitors (Figure 4).

Each contribution of R1 parts as ER chemical features to the inhibitory activity was calculated in the topomer CoMFA

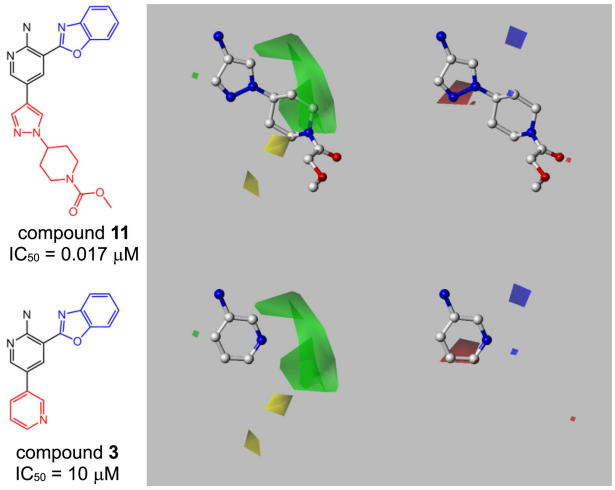

Figure 4. The contour maps of Topomer CoMFA model for active and inactive compounds. Green and yellow contours highlight favored and disfavored steric bulk groups, whereas red and blue contours highlight favored negative and positive electrostatic interactions, respectively.

model (Table 1). For two core part, 3-(benzo[*d*]oxazol-2-yl)pyridine-2-amine and 3-(1-(2,6-dichloro-3-fluorophenyl)-ethoxy)pyridine-2-amine, the correlation coefficients, r^2 between experimental pIC_{50} and contribution of R1 part are 0.670 and 0.913, respectively as shown in Figure 5. As mentioned above, if compound **8** were excluded as an outliner, the r^2 could increase to 0.883. The R1 part of active compound **11** highly contributed to its inhibitory activity with 3.81 value, while that of inactive compound **3** showed the low contribution with 0.89 value. Consequentially, we confirmed that ER chemical features of c-Met inhibitors are closely related with the inhibitory potency to the target as well as chemical features of known other regions, but there is only the hydrophobic interaction.

Caballero *et al.* also analyzed ER chemical features of c-Met inhibitors, which showed that occupancy of ribose pocket has a negative effect on the inhibitory activity for 4-(4-amino-2-fluorophenoxy)-2-pyridinyl amines (AFPP) and 3-fluoro-4-(1*H*-pyrrolo[2,3-*b*]pyridin-4-yloxy) anilines (FPPA), but a positive effect on the inhibitory activity for 3-fluoro-4-(pyrrolo[2,1-*f*][1,2,4]triazin-4-yloxy)anilines (FPTA).[12] These results for AFPP and FPPA are in contrast to our results because substituents on the 4 position of AFPP and FPPA are located in more closely p-loop or flexible regions than those on the 5 position of pyridine-2-amine in our compounds, so steric hindrances of former have a negative effect on their inhibitory activities. However, the substituents of FPTA face toward the hydrophobic cleft in the outside of active site, in which steric bulk or hydrophobic groups show a positive effect on the inhibitory activity such as our results. They also have shown that substituents of hydrophobic groups would be favorable for its activity at the external region by using the comparative molecular similarity analysis (CoMSIA) and multiple linear regression (MLR) with topological vectors. Although they suggested the H-bond interaction including Asp1164 as a dominant positive effect, in our studies hydrophobic interactions were identified as a main effect on the inhibitory activities of compounds.

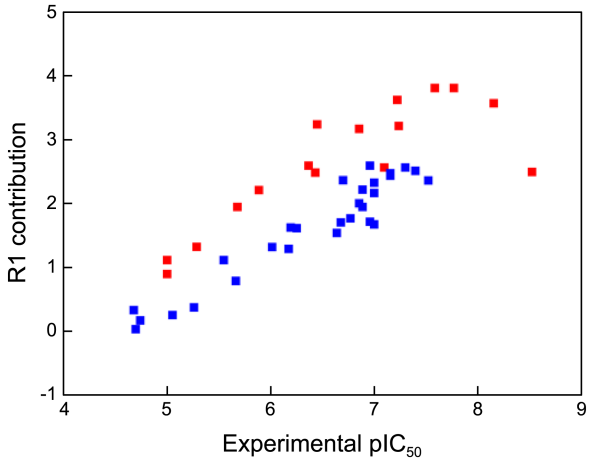

Figure 5. The correlations between their experimental pIC_{50} and contribution of R1 part for two core parts: 3-(benzo[*d*]oxazol-2-yl)pyridine-2-amine (■) and 3-(1-(2,6-dichloro-3-fluorophenyl)-ethoxy)pyridin-2-amine (■).

Conclusion

In this study, the 3D-QSAR studies on ER chemical features of pyridine-2-amines were conducted using docking, CoMFA, and topomer CoMFA methods, of which the statistical results were good in terms of q^2 and r^2, and showed high predictive abilities for the test set. The results suggested that the more ER chemical features of pyridine-2-amines are hydrophobic groups, the more the inhibitory potency to the target enhances, which can be interpreted by the hydrophobic cleft formed by the side chains of Ile1084 and Tyr1159 and the backbones of Lys1161, His1162, Gly1163, and Asp 1164. Further we have tried to seek 3-(benzo[*d*]oxazol-2-yl)pyridine-2-amines with the structural modification focused on chemical features in the central and allosteric regions of c-Met active site.

Acknowledgments. This study was supported by grant TS131-18R (TS121-22) from the Ministry of Knowledge Economy (Dr. Chae).

References

1. Trusolino, L.; Bertotti, A.; Comoglio, P. M. *Nat. Rev. Mol. Cell Biol*. **2010**, *11*, 834.
2. Eder, J. P.; VandeWoude, G. F.; Boerner, S. A.; LoRusso, P. M. *Clin. Cancer Res*. **2009**, *15*, 2207.
3. Puri, N.; Ahmed, S.; Janamanchi, V.; Tretiakova, M.; Zumba, O.; Krausz, T.; Jagadeeswaran, R.; Salgia, R. *Clin. Cancer Res*. **2007**, *13*, 2246.
4. Mazzone, M.; Comoglio, P. M. *FASEB J*. **2006**, *20*, 1611.
5. Huh, C. G.; Factor, V. M.; Sánchez, A.; Uchida, K.; Conner, E. A.; Thorgeirsson, S. S. *Proc. Natl. Acad. Sci. U.S.A*. **2004**, *101*, 4477.
6. Birchmeier, C.; Birchmeier, W.; Gherardi, E.; Vande Woude, G. F. *Nat. Rev. Mol. Cell Biol*. **2003**, *4*, 915.

7. Matsumoto, K.; Nakamura, T. *Cancer Sci*. **2003**, *94*, 321.
8. Trusolino, L.; Comoglio, P. M. *Nature Rev. Cancer* **2002**, *2*, 289.
9. Christensen, J.; Burrows, J.; Salgia, R. *Cancer Lett*. **2005**, *225*, 1.
10. Asses, Y.; Leroux, V.; Tairi-Kellou, S.; Dono, R.; Maina, F.; Maigret, B. *Chem*. *Biol*. *Drug Des*. **2009**, *74*, 560.
11. Larsen, C. A.; Bisson, W. H.; Dashwood, R. H. *J. Med. Chem*. **2009**, *52*, 6543.
12. Caballero, J.; Quiliano, M.; Alzate-Morales, J. H.; Zimic, M.; Deharo, E. *J. Comput*. *Aided Mol*. *Des*. **2011**, *25*, 349.
13. Cho, S. Y.; Han, S. Y.; Ha, J. D.; Ryu, J. W.; Lee, C. O.; Jung, H. J.; Kang, N. S.; Kim, H. R.; Koh, J. S.; Lee, J. K. *Bioorg. Med. Chem*. *Lett*. **2010**, *20*, 4223.
14. Lee, J. K.; Han, S. Y.; Jung, H. J.; Yang, J.; Choi, J. W.; Chae, C. H.; Park, C. H.; Choi, S. U.; Lee, K. H.; Ha, J. D.; Lee, C. O.; Ryu, J. W.; Kim, H. R.; Koh, J. S.; Cho, S. Y. *Bioorg*. *Med*. *Chem*. *Lett*. **2012**, *22*, 4044.
15. Cui, J. J.; Tran-Dubé, M.; Shen, H.; Nambu, M.; Kung, P.-P.; Pairish, M.; Jia, L.; Meng, J.; Funk, L.; Botrous, I.; McTigue, M.; Grodsky, N.; Ryan, K.; Padrique, E.; Alton, G.; Timofeevski, S.; Yamazaki, S.; Li, Q.; Zou, H.; Christensen, J.; Mroczkowski, B.; Bender, S.; Kania, R. S.; Edwards, M. P. *J. Med. Chem*. **2011**, *54*, 6342.
16. Copeland, R. A.; Lombardo, D.; Giannaras, J.; Decicco, C. P. *Bioorg*. *Med*. *Chem*. *Lett*. **1995**, *5*, 1947.
17. Pipeline Pilot, version 8.5; software for thechnical computation; Accelrys Inc.: St. San Diego 2012.
18. Schrödinger, release 2013; software for technical computation; Schrödinger, LLC: New York, NY 2013.
19. Kaminski, G. A.; Friesner, R. A.; Tirado-Rives, J.; Jorgensen, W. J. *J. Phys*. *Chem*. *B* **2001**, *105*, 6474.
20. Friesner, R. A.; Banks, J. L.; Murphy, R. B.; Halgren, T. A.; Klicic, J. J.; Mainz, D. T.; Repasky, M. P.; Knoll, E. H.; Shaw, D. E.; Shelley, M.; Perry, J. K.; Francis, P.; Shenkin, P. S. *J. Med. Chem*. **2004**, *47*, 1739.
21. Halgren, T. A.; Murphy, R. B.; Friesner, R. A.; Beard, H. S.; Frye, L. L.; Pollard, W. T.; Banks, J. L. *J. Med. Chem*. **2004**, *47*, 1750.
22. Friesner, R. A.; Murphy, R. B.; Repasky, M. P.; Frye, L. L.; Greenwood, J. R.; Halgren, T. A.; Sanschagrin, P. C.; Mainz, D. T. *J. Med. Chem*. **2006**, *49*, 6177.
23. SYBYL-X, version 2.0; software for technical computation; Tripos Inc.: St. Louis 2012.